ACS OMEGA

http://pubs.acs.org/journal/acsodf

Article

Research on Optimal Blocking Limits and Injection Parameter Optimization of Polymer Microsphere Conformance Control

Wenyue Zhao, Juan Ni, Ganggang Hou, Yuqin Jia, Pengxiang Diwu, Xinyu Yuan, Tongjing Liu,* and Jirui Hou

Cite This: *ACS Omega* 2021, 6, 8297−8307

Read Online

ACCESS | Metrics & More | Article Recommendations

ABSTRACT: Polymer microsphere (PM) profile control has been attributed to improving sweep efficiency during the oil development process. The critical factors for PM conformance control are the plugging properties controlled by matching the relationship between the throat diameter and particle size and the injection parameters. A new matching relationship between the reservoir and PM based on the function of blocking rate and the ratio of throat diameter to microsphere diameter (C_R) is established to choose the most appropriate PM size. The blocking rate indicates that it will get the most excellent plugging effect when C_R is 0.5. The displacement experiments under different injection concentrations and other injection volumes show that the blocking rate is increased by injection concentration and finally stabilized. A similar trend is presented between the injection volume and plugging rate. The optimal injection concentration is 0.5%, and the optimal injection volume is 0.3 PV. According to the new size selection method and injection parameter optimal method, PM100 chooses to conduct field application. PM100 presents a good performance with a success rate of 37.5% and a validity period of more than 120 days, and its daily oil production rate increased 1.7 times, on average, and finally, the total oil increase is 556 t. The optimal size microsphere shows a good EOR effect, which indicates that this size selection method is reasonable.

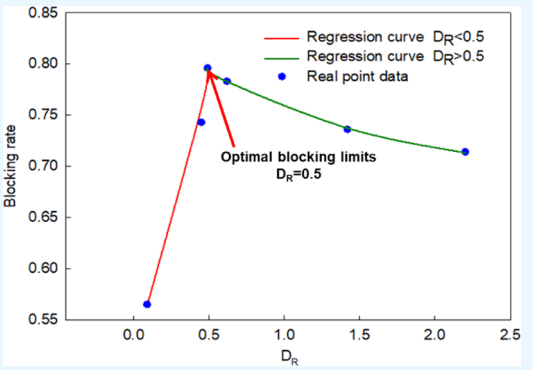

1. INTRODUCTION

Heterogeneity of the low-permeability reservoir is quite severe, and the displacement profile is inconsistent in water flooding (WF) development, which affects the effect of WF.[1−3] During WF development, injected water rushes along the dominant percolation direction as the existing microcracks in the reservoir, which is easy to lead to water breakthrough and stable production period shortening.[4−6] Unlike the chain-like polymer that is repeatedly connected by specific structural units, polymer microspheres (PMs) are spherical polymer composite materials with diameters ranging from nanometers to micrometers, high specific surface area, high reactivity, and other unique physical, chemical, and biological properties.[7] As a kind of profile adjustment material with good salt tolerance, the PM maintains good conformance control ability.[8−10] The PM is characterized by plugging, deformation, migration, and second plugging. It has a practical ability to improve formation heterogeneity and stop or slow down the injected water one-way rush.[11,12] It can also reduce the increasing water cut rate in the water breakthrough wells and has double functions of profound profile control and oil displacement. Increasing the swept volume of injected water can achieve long-term oil displacement from the water well to oil well and the ultimate goal of enhanced recovery.[13,14] Deep conformance control technology of the PM has been applied to Bohai, Shengli, Changqing, and other oilfields and achieved good results.[15−19]

The matching relationship between the particle size of the microspheres and the throats' diameter determines the PM's conformance control performance. When PMs are large, the particles can only block the oil layer near the water well. Quickly, the injected water will flow around and enter the high-permeability layer again. The wrong PM size causes the failure to play a role in conformance control. If the particle size of the PMs is small, the conformance control measures cannot achieve the desired performance, and the blocked channel is prone to channeling again.[20,21]

The method of determining the particle size of the microspheres is to select the particle size in the recommended matching coefficient range according to the ratio between the

Received: January 1, 2021
Accepted: March 4, 2021
Published: March 16, 2021

https://dx.doi.org/10.1021/acsomega.1c00009
ACS Omega 2021, 6, 8297−8307

Table 1. Ion Content of Formation Water

composition	Na+ + K+	Mg^{2+}	Ga^{2+}	Cl^{-}	SO_4^{2-}	HCO_3^{-}
concentration/mg/L	24,685	727	9585	45,480	486	182

particle size of the PMs and the reservoir's throat diameter.[22,23] The most widely used, in recent years, is the three-ball bridging theory. When the particle size is greater than or equal to 1/3 of the formation throat, it can form an effective blockage.[24] Since engineers applied the view to the petroleum industry, this theory has always been the primary guiding principle for selecting polymer bridge particle size. Scientific researchers have optimized the selection range of PM size of 1/7−2/3 of the throat diameter.[25] The field application determines the particle size of the microspheres within the scope of the matching coefficient. The selected microspheres can form a blockage, but we do not know whether it can create an optimal blocking. When using PMs for in-depth conformance control, it is necessary to select microspheres with a particle size that can form the optimal plugging to achieve the best profile control performance. The most appropriate PMs require the optimal matching coefficient, so we should clarify the matching coefficient to form the highest blocking rate. This paper intends to figure out the optimal matching coefficient to optimize the size selection of PMs.

In this paper, we select two kinds of PMs applied in Changqing Oilfield to conduct the microsphere hydration experiment to evaluate the expansion performance. Natural core displacement experiments with different hydration degrees of PMs are conducted to analyze the blocking performance. We aim to establish a matching coefficient formula between the ratio of PM particle size to throat diameter and blocking rate to clarify the optimal matching coefficient by analyzing the experiments' results. We also studied the optimal injection concentration and the total injection volume by displacement experiments with different injection concentrations and injection volumes. Finally, a field application was carried out to evaluate conformance control performance and verify the optimal matching coefficient's feasibility.

2. EXPERIMENTAL CONDITION

2.1. Materials. *2.1.1. Polymer Microspheres.* In this research process, two kinds of PMs are studied with the calibration diameter as 100 nm (PM100) and 800 nm (PM800) separately. These two kinds of microspheres have been applied in Changqing Oilfield with good performance.[26] Also, according to the throat diameter and the particle size of these two kinds of PMs, the calculated matching coefficient is within the recommended matching coefficient range. PMs are synthesized by reverse-phase emulsion polymerization from Xi'an Changqing Chemical Industry Group Co. LTD. Environmentally friendly PMs are nontoxic, noncorrosive, and kept in white oil with a sufficient content of 20%. We use anhydrous ethanol (CH_3CH_2OH) as the dispersion medium to make a uniform dispersion solution of PMs in the initial state. PMs are easily spread around uniformly in water and skillfully injected into the core with viscosity close to that of water.

2.1.2. Brine. Changqing Oilfield provides the formation water, and its ion composition analysis results are shown in Table 1. The simulated brine with a salinity of 81,145 mg/L is prepared according to ion content composition by adding inorganic salts into distilled water. The simulated brine is used to prepare PM-dispersed solution from property evaluation experiments to plugging experiments. The simulated brine ion composition is presented in Table 1.

2.1.3. Cores. With the gradual decrease in the number of natural cores in oil and gas fields, it is increasingly challenging to find cores that can be used for comparison and repeated experiments. Using artificial cores to replace natural cores for indoor simulation experiments has become an effective way to solve this problem.[27−29] Compared with artificial cores, natural cores are closer to underground reservoir rocks in the pore structure, which can genuinely reflect the pore structure's influence on the percolation process. The pore structure is essential to the stacking method and stacking probability and significantly impacts the blocking rate in the PM conformance control. Ten natural cores of nearly the same size are used in plugging experiments. These natural cores have similar properties that the air permeability of natural cores ranges from 15.4 to 16.2 mD and the porosity ranges from 15.19 to 15.75%. Cores 1# to 3# are used to carry out PM100 plugging experiments at the different swelling times. Cores 4# to 6# are used to carry out PM800 plugging experiments at the different swelling times. Cores 7# and 8# are used to carry out plugging experiments of the 100 nm PM at different concentrations. Cores 9# and 10# are used to carry out plugging experiments of the 100 nm PM at different inject volumes. The key parameters are shown in Table2.

Table 2. Key Parameters of Cores

core number	length/cm	diameter/cm	porosity/%	permeability[a]/mD
1#	10.023	2.515	15.75	15.5
2#	10.039	2.515	15.42	15.9
3#	10.011	2.515	15.18	16.0
4#	10.055	2.515	15.24	15.4
5#	10.057	2.515	15.23	16.2
6#	10.005	2.515	15.19	16.0
7#	10.077	2.515	15.36	15.9
8#	10.048	2.515	15.25	16
9#	10.028	2.515	15.46	15.9
10#	10.003	2.515	15.28	16

[a]Air logging permeability.

2.2. Apparatuses. The size of PMs is tested using an ultrasonic instrument (produced by Tianjin Auto science Instrument Co., Ltd.) and nanoparticle size analyzer (built by Beckman Coulter, USA). The ultrasonic instrument is primarily used to make PM solution dispersed uniformly with an ultrasonic frequency of 40 KHz and an ultrasonic power of 120 W. The nanoparticle size analyzer with a measuring range of 0.6 nm to 7 μm is mainly applied to measure size distribution. Other applications including thermostats, quartz cuvettes (10 mL), and electromagnetic stirrers are also applied in these experiments.

The displacement device is used during the process of plugging property evaluation. Instruments such as a double-tank constant speed constant pressure pump, core holder, intermediate container, constant temperature system, pressure

https://dx.doi.org/10.1021/acsomega.1c00009
ACS Omega 2021, 6, 8297−8307

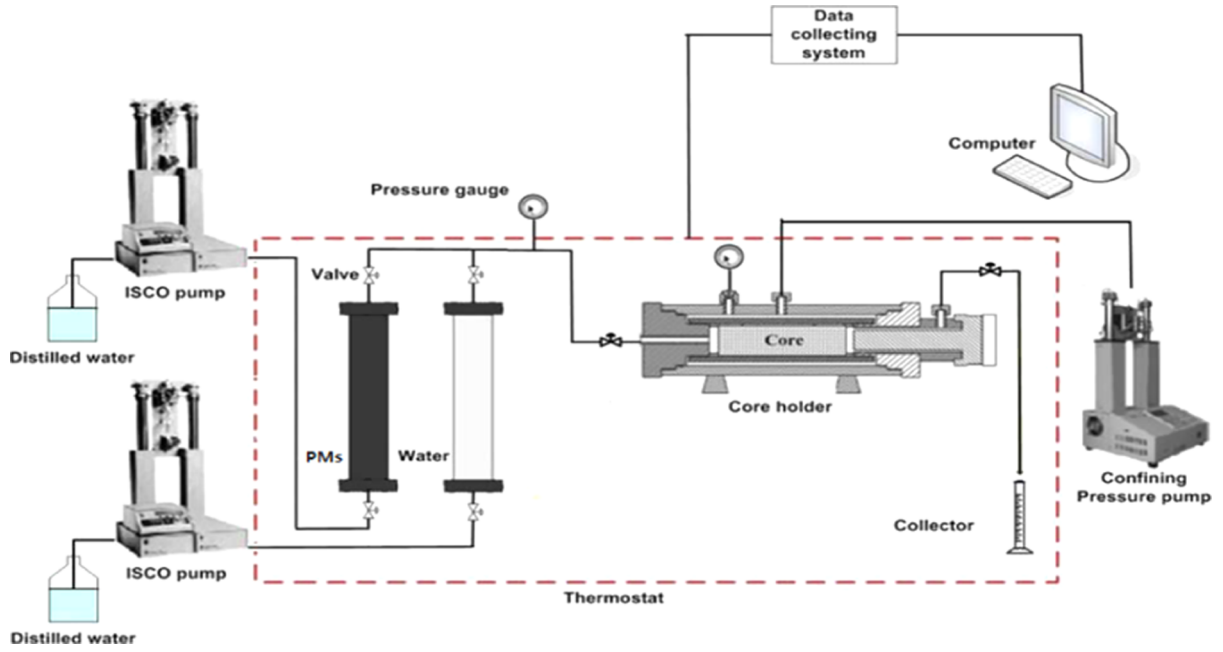

Figure 1. Displacement equipment and process diagram.

Table 3. Key Parameters and Experimental Scheme

PM	core number	injection concentration/%	injection volume/PV	injection velocity/mL/min	swelling time/d
PM100	1#	0.3	0.3	0.3	0
	2#				6
	3#				15
PM800	4#	0.3	0.3	0.3	0
	5#				6
	6#				15

measuring device, and displacement experiment device are used to inject the PCE solution into the core. The experimental equipment and process are shown in Figure 1.

2.3. Experimental Methods. *2.3.1. Hydration Swelling Experiment.* The PMs are characterized by plugging high-permeability zones and migrating into the deep part of the formation to improve sweeping water volume.[30] We conduct hydration experiments to evaluate the swelling properties by measuring the diameter distribution to analyze the PM's changing law.[31,32] PM hydration swelling property evaluation is mainly run using an ultrasonic instrument and nanoparticle size analyzer.[33]

The PM solution was prepared to measure the size distribution. First, in the process of PM solution preparation for testing initial particle size distribution, a certain amount of microsphere sample was dripped into anhydrous ethanol to prepare a 100 mL microsphere solution with a mixing speed of 400 rpm for 30 min using an ultrasonic instrument. Immediately after mixing, the anhydrous ethanol microsphere solution was sucked into a dropper, and the particle size distribution was measured using a laser particle size analyzer (Microtrac S3500). We measure size distribution three times on a sample and take the average as the initial particle diameter. Then, we disperse QY in simulated formation water and place it in the thermostat at 70 °C. It was shaken for 30 min in an ultrasonic instrument for uniform dispersion and measure particle size three times every 24 h. At last, we obtain the particle size distributions with the different periods of aging. The expansion ratio was calculated using eq 1 to evaluate the hydration swelling properties[34]

$$E_R = \frac{D_2}{D_1} \quad (1)$$

where E_R is the expansion ratio and D_1 and D_2 are the mean diameters of the PMs at the initial state and after expansion, respectively, nm.

2.3.2. Plugging Ability at Different Swelling Time. This study uses 1# to 6# natural cores to evaluate the influence of hydration swelling on plugging properties. PM100 and PM800 injection schemes include an injection concentration of 0.3%, an injection volume of 0.3 PV, and an injection velocity of 0.3 mL/min. We inject the PM solution to the core at the different aging periods (0, 6, and 15 days) and conduct these experiments at a temperature of 70 °C. Table 3 shows the key parameters and experimental scheme of natural cores of 1# to 6#.

Before conducting WF, we weight the cores after drying in the thermostats. Then, we vacuumed the cores for 3 h and saturated them with simulated brine, and we calculate the core porosity with the difference between the mass. Subsequently, we adjust the thermostat's temperature to 70 °C. We inject the simulated formation water into cores at a rate of 0.3 mL/min until the injection pressure becomes stable. We gain the core permeability through the recording pressure. After that, we inject PM-dispersed solution at a different swelling time into cores at a rate of 0.3 mL/min, and the cumulative injection

https://dx.doi.org/10.1021/acsomega.1c00009
ACS Omega 2021, 6, 8297−8307

volume is 0.3 PV. This process is PM flooding (PMF). The last displacement process is subsequent water flooding (SWF). The simulated formation water is injected into cores at a rate of 0.3 mL/min until the injection pressure is stable. The pressure changes and the absolute permeability in the whole experiment are measured.

In this work, the resistance coefficient and blocking rate are calculated using eqs 2 and 3. The retention rate of the PMs in the core is calculated using eq 4[26]

$$F_r = \frac{\lambda_w}{\lambda_p} = \frac{\left(\frac{K}{\mu}\right)_w}{\left(\frac{K}{\mu}\right)_p} = \frac{\Delta P_p}{\Delta P_w} \times \frac{Q_w}{Q_p} \quad (2)$$

$$\eta = 1 - \frac{K_{sw}}{K_w} \quad (3)$$

where F_r is the resistance coefficient and η is the blocking rate; K_w, K_p, and K_{sw}, respectively, represent the core permeability after WF, PMF, and SWF, μm^2; μW and μ_p are the viscosity of water and the PM system, respectively, mPa·s; DPW and DPP represent the differential pressure of WF and PMF, respectively, MPa; Q_w and Q_p are the injection rate during WF and PMF, respectively, mL/min.

2.3.3. Injection Concentration. Another two natural cores 7# and 8# are used to optimize injection concentration of the PM. PM100 after aging for 15 days is injected into cores at an injection velocity of 0.3 mL/min and an injection volume of 0.3 PV. The injection concentration of 7# and 8# cores is 0.1 and 0.5%, separately. Combined with the 3# core experiment, the overall experiment scheme of injection concentration is shown in Table4.

Table 4. Experimental Scheme of Injection Concentration

PM	core number	injection volume/PV	injection velocity/mL/min	injection concentration/%
PM100	7#	0.3	0.3	0.1
	3#			0.3
	8#			0.5

2. 3. 4. Injection Volume. Natural cores 9# and 10# are used to conduct injection volume optimization experiments. PM100 PMs are injected after aging for 15 days into cores at an injection velocity of 0.3 mL/min and a concentration of 0.3%. The injection volume of 9# and 10# cores is 0.1 and 0.5 PV, separately. Combined with the 3# core experiment, the overall experiment scheme of injection concentration is shown in Table5.

3. RESULTS AND DISCUSSION

3.1. Swelling Property Analysis. PM100 and PM800 are dispersed in ethyl alcohol to measure the initial state's average diameter at 25 °C. Then, we distribute PM100 and PM800 in simulated brine with a salinity of 81145 mg/l and put it into the thermostat at 70 °C. The PM's particle size distribution is measured every 24 h and continuously measured for 19 days.

Table 5. Experimental Scheme of the Injection Volume

PM	core number	injection concentration/%	injection velocity/mL/min	injection volume/PV
PM100	9#	0.3	0.3	0.1
	3#			0.3
	10#			0.5

Particle average size measurement results of PM100 microsphere are shown in Table 6. The expansion ratio is calculated according to eq 1 and shown as in Figure 2. It can be found that with increased swelling time, particle size and expansion ratio gradually increases and finally tended to be stable. The initial average particle size of PM100 is 165 nm and then reached 583 nm after 3 days of swelling, which expanded by 3.5 times. The average particle size increased to 904 nm after 9 days of hydration, and it grew by 5.5 times. After hydration time reached 13 days, particle size tended to be stable.

The particle size distributions on the initial state and swelling equilibrium state are shown in Figure 3. It can be seen that PM-dispersed solution is an extremely heterogeneous discontinuous phase system. From the initial state to swelling equilibrium state, particle size distribution shows a noticeable right shift. After expansion, the average size of PM100 is 1140 nm and expanded by 6.9 times. The increase in PM size illustrated that PM100 has a suitable swelling property.

The average size and expansion ratio of PM800 are shown in Table 7 and Figure 4. The results show that particle size gradually increased with increased swelling time and finally tended to be stable. The average particle size of PM800 at the initial state is 884 nm, and after 3 days of swelling, the particle diameter reaches 1786 nm. Average particle size increased to 3255 nm after swelling for 9 days and expanded by 4.2 times. After swelling for 14 days, the average particle size shows no apparent increase and gets to a swelling equilibrium state.

Figure 5 shows the size distribution of PM800 at the initial state and swelling equilibrium state. We found that from the initial state to the swelling equilibrium state, particle size distribution shows a slightly right shift. After expansion, the average size of PM800 is 4017 nm and expanded by 5.1 times.

3.2. Matching Relationship Between the PM and Reservoir. In the plugging property evaluation experiment, cores 1# to 3# are used in PM100 displacement experiments. This study uses cores 4# to 6# to conduct PM800 displacement experiments. The injection pressure curves of PM800 and M100 with aging for 0, 6, and 15 days are shown in Figures 6 and 7. Flooding pressures of PM100 and PM800 at the end of WF, PMF, and subsequent water flooding (SWF) are shown in Table 8. The resistance coefficient and blocking rate calculated using eqs 2 and 3 are presented in Table 9.

Figure 6 shows that the injection pressure of PM100 is increasing obviously in a stepped way after PMF. By comparing injection pressure under different swelling times, the initial injection pressure of WF is about 95 KPa, and injection pressure increased slightly from 100 to 120 KPa. However, the injection pressure of SWF increased obviously from 175 to 380 KPa. Flooding pressures of PM100, at the end of WF, PMF, and SWF, are shown in Table 8. For PM100, with increasing swelling time, the resistance coefficient increases from 2.9 to 4.22 and the blocking rate increases from 0.655 to 0.783.

Figure 7 shows the relationship between the injection volume and an injection pressure of the PM800 microsphere plugging experiment. It can be found that with increasing injection volume, injection pressure increased. After injection of the PM, injection pressure increased obviously in a stepped way. For the PM800 microsphere, stable WF pressure was

https://dx.doi.org/10.1021/acsomega.1c00009
ACS Omega 2021, 6, 8297−8307

Table 6. PM100 Average Diameter at Different Swelling Times

time/d	0	1	2	3	4	5	6	7	8	9
D^a/nm	165	393	516	583	670	768	826	852	872	904
time/d	10	11	12	13	14	15	16	17	18	19
D^a/nm	965	1064	1116	1140	1140	1142	1180	1178	1185	1185

[a]PM100 particle diameter.

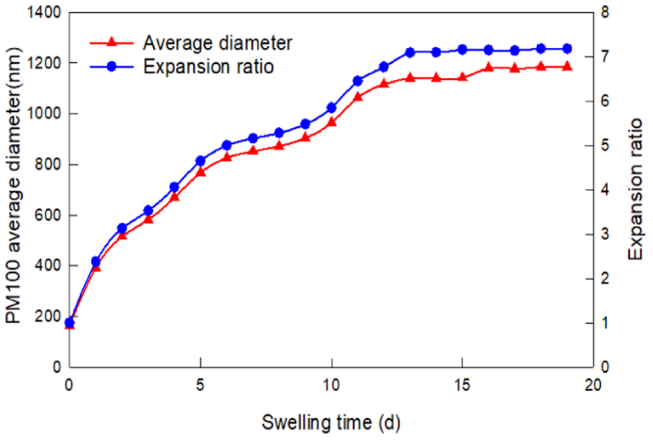

Figure 2. PM100 PM relationship between the microsphere size, expansion ratio, and swelling time.

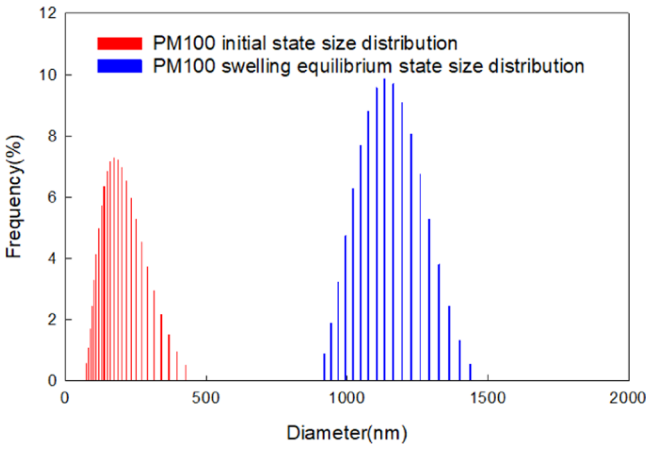

Figure 3. 100 nm particle size distribution at the initial state and swelling equilibrium state.

slightly different. The injection pressure of 0 day hydration is relatively large at 120 KPa, and the injection pressures of 6 days of hydration and 15 days of hydration are about 90 KPa. With increased hydration time, stable pressure of SWF of PM800 increased and then decreased. The steady pressure of SWF decreased from 380 KPa in 6 days of hydration to 315 KPa in 15 days of hydration. According to the analysis of SWF stable pressure, plugging performance of microspheres after 15 days of hydration was worse than that after 6 days of hydration. Table 9 shows that the resistance coefficient and blocking rate of PM800 decreased with increased hydration time, the resistance coefficient fell from 4.92 to 3.5, and the blocking rate dropped from 0.796 to 0.714. The falling of the resistance coefficient and plugging rate indicates reducing plugging ability with increasing size of PM800.

The plugging analysis results show that both PM100 and PM800 could form effective plugging in cores. However, the blocking rate of these two kinds of PMs after swelling is significantly different in that PM100 plugging strength increases and PM800 blocking strength decreases by increasing aging time. The main difference between the initial state and after swelling was the particle size. By analyzing the change law of sealing rate with the particle size ratio to pore throat diameter, the optimal particle size selection method is obtained in microsphere deep profile control.

At present, the Carman−Kozeny equation is commonly used to calculate the throat's diameter, shown in eq 4.

$$r = \sqrt{\frac{8K}{\phi}} \tag{4}$$

where K is the effective permeability of the rock, μm^2; Φ is formation porosity; r is the average radius of the throat, μm; and τ is tortuosity of the throat. The ratio of the PM diameter to the diameter is as follows

$$D_R = \frac{D_P}{D_C} \tag{5}$$

$$D_C = 2r \tag{6}$$

D_R is the PM diameter ratio to the diameter; D_C is the throat diameter, nm; and D_P is the PM diameter, nm. D_C and D_R are calculated with eqs 4−6. The calculating results and average diameter of PM100 and PM800 are shown in Table 9 and Figure 8.

According to Table 9, for the PM100 microsphere, with an increase in particle size ratio to pore throat diameter, the plugging rate increased. For the PM800 microsphere, with increased hydration time, the particle size ratio to the pore throat diameter increased, while the plugging rate decreased gradually. D_R at PM100 hydration equilibrium was similar to D_R at 0 day swelling of PM800, and the blocking rate is also identical. Through comprehensive analysis of PM100 and PM800 plugging rates with D_R, it can be seen that when D_R < 0.5, the blocking rate increases rapidly but decreases slowly when D_R > 0.5. The correlation between D_R and the blocking rate is presented as eq 7. D_R < 0.5 blocking rate is

Table 7. PM800 Average Diameter at Different Aging Times

time/d	0	1	2	3	4	5	6	7	8	9
D^a/nm	884	931	1496	1786	2015	2231	2615	2886	3061	3255
Time/d	10	11	12	13	14	15	16	17	18	19
D^a/nm	3353	3548	3717	3940	4017	4034	4046	4052	4056	4064

[a]PM800 particle diameter.

https://dx.doi.org/10.1021/acsomega.1c00009
ACS Omega 2021, 6, 8297−8307

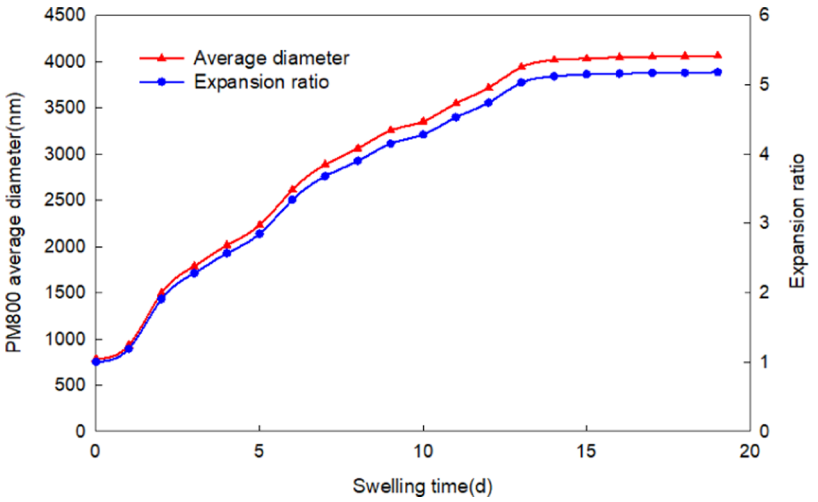

Figure 4. PM800 relationship between microsphere size, expansion ratio, and hydration time.

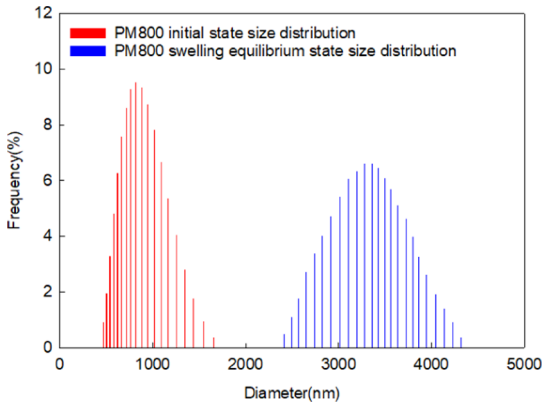

Figure 5. PM800 particle size distribution at the initial state and swelling equilibrium state.

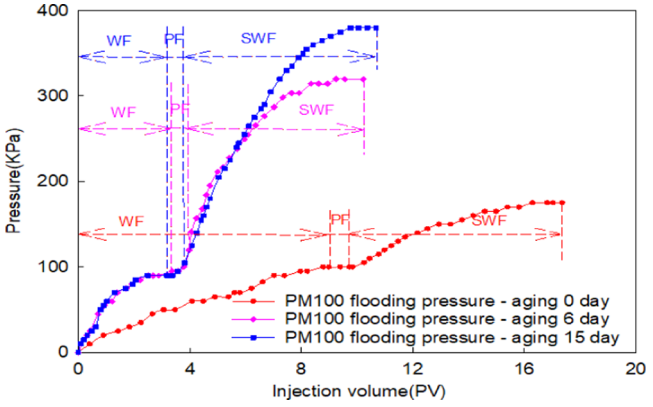

Figure 6. PM100 relationship between the injection volume and injection pressure.

exponentially related to D_R and is logarithmic to D_R when $D_R > 0.5$.

It is believed that there is an optimal D_R value that maximizes the plugging rate. Therefore, the optimal particle size of the microsphere is 0.5 times the throat diameter.

$$\eta = \begin{cases} 0.524\, e^{0.8189 D_R} & D_R < 0.5 \\ -0.055 \ln(D_R) + 0.7565 & D_R > 0.5 \end{cases} \quad (7)$$

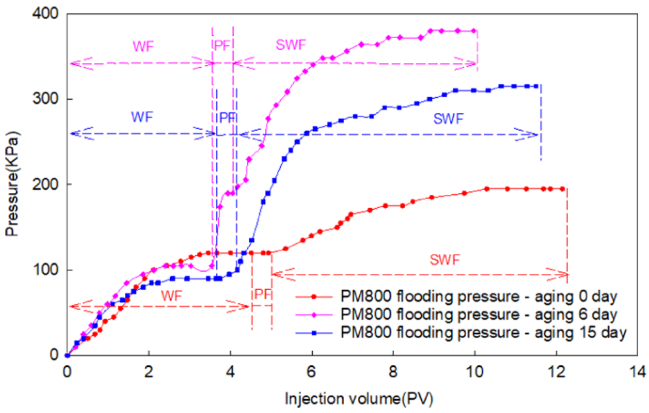

Figure 7. PM800 relationship between the injection volume and injection pressure.

Table 8. Differential Pressure as a Function of Pore Volume Injected

PM	aging time/Day	WF	PMF	SWF
PM100	0	90	100	175
	6	95	120	320
	15	90	125	380
PM800	0	120	125	195
	6	95	105	380
	15	90	95	315

Table 9. Ratio of the PM Diameter to the Diameter and Blocking Rate

PM	aging time/d	D_P/nm	D_C/nm	D_R	F_r	η
PM100	0	165	1774.60	0.09	2.9	0.655
	6	826	1816.48	0.45	3.47	0.723
	15	1142	1836.53	0.62	4.22	0.783
PM800	0	884	1798.22	0.49	4.92	0.796
	6	2615	1844.94	1.42	3.95	0.747
	15	4034	1835.93	2.20	3.5	0.714

When D_R is less than 1/3, it is considered that the microspheres form a blockage at the throat by bonding. As the particle size of the microspheres increases, the blocking mechanism becomes bridging, and the microspheres form straining when the particle size further increases. According to

https://dx.doi.org/10.1021/acsomega.1c00009
ACS Omega 2021, 6, 8297−8307

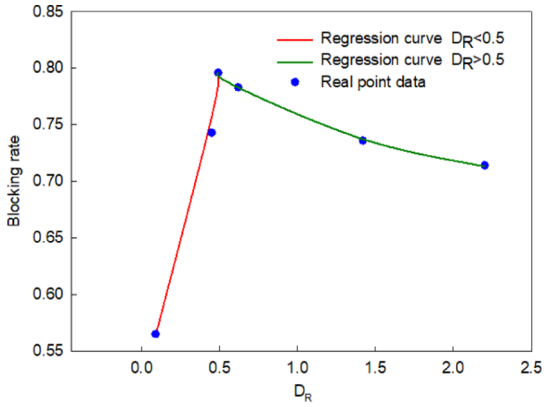

Figure 8. Differential ratio of PM diameter to throat diameter as a function of blocking rate.

the experimental results of plugging capacity, it is found that the plugging capacity of the adhesive is weaker than bridging. When the same concentration and the same injection volume are used, the blocking strength of bridging is more considerable, and the probability of effective blocking is larger than adhesive blocking. Therefore, the blocking rate is higher, and a better blocking effect is seen. When D_R is more significant than 0.5, microspheres tend to form strain blocking. Because the particle size of the microsphere is too large, it is difficult to pass through the throat with a small diameter, and the ability to migrate deep into the reservoir is lost. The blocking range of the microspheres is relatively small, and the apparent result is that the blocking ability becomes poor. Under the premise of ensuring inject ability, as the particle size increases, the blocking rate gradually decreases and eventually stabilizes. The changing trend is because the range of microspheres that can be blocked is no longer changed, and the number of throats that can be blocked is balanced, so the blocking rate is unchanged.

3.3. Injection Concentration. The experiment uses PM100 microspheres on the 15th day of hydration, the injection volume is 0.3 PV, and the injection velocity is 0.3 mL/min. The blocking rate at different concentrations obtained from the displacement experiment is shown in Figure 9. We found that the blocking rate is increased by injection concentration and finally stabilized. The changing trend of the blocking rate is because bridging requires a certain number of microspheres to pass through the throat at the same time. At low concentrations, fewer microspheres pass through the throat simultaneously which lead to a small probability of bridge forming and a low blocking rate. As the concentration increases, the likelihood of bridge plugging increases, but when the concentration reaches the critical value for forming an effective plugging, the plugging rate reaches the maximum value. When the microsphere concentration increases, the plugging rate will not increase and tend to be stable.

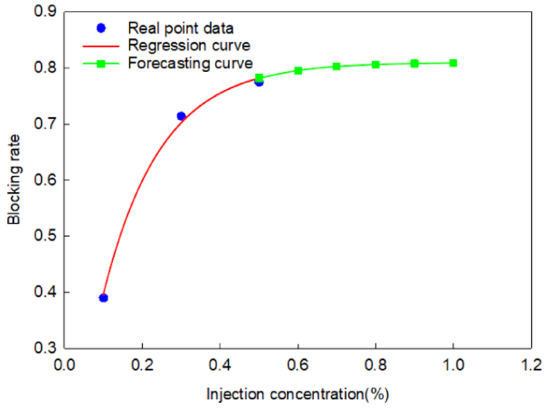

Figure 9. Differential ratio of PM diameter to throat diameter as a function of blocking rate of PM100 and PM800.

By fitting the plugging rate and injection concentration data, it is found that the two satisfy the relationship shown in eq 8 below. According to the prediction result, we can find that when the concentration is more significant than 0.5%, the plugging rate increase is minimal. Also, a high concentration of microsphere solution causes uneven dispersing. Therefore, considering the plugging capacity and the solution preparation condition, it is believed that 0.5% is the optimal injection concentration.

$$\eta = 0.8103(1 - 0.0012^{c_p}) \quad (8)$$

3.4. Injection Volume. PM100 is injected on the 15th day of hydration with a concentration of 0.3% and an injection velocity of 0.3 mL/min. The blocking rate at different concentrations obtained from the experiment is shown in Figure 10. Figure 10 indicates that the blocking rate increases with injection volume and is finally stabilized. As the injection volume increases, the number of blocked throats increases. As the injection amount further increases, the pores and throats that can be blocked have been entirely blocked, so even when we continued to increase the injection volume, the plugging rate will not increase. Eventually, the plugging rate tends to stabilize.

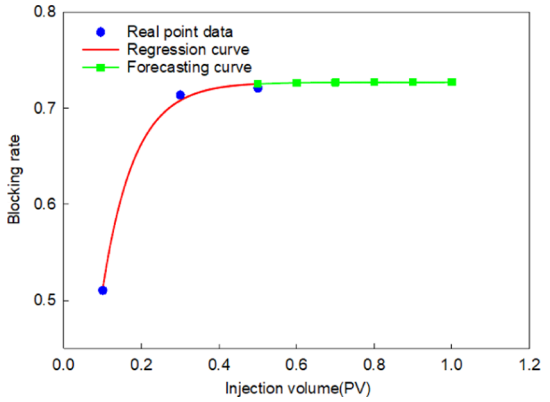

Figure 10. Differential ratio of PM diameter to throat diameter as a function of blocking rate of PM100 and PM800.

We can find that the blocking rate and injection volume satisfy the following functional relationship by fitting the experimental data, shown in eq 9. According to the prediction results, it can be concluded that when the injection volume of the microspheres is greater than 0.3 PV, the blocking rate increase is tiny, and the high injection volume will further increase the cost. By considering the measure's cost, 0.3 PV is viewed as the limit injection volume for profile control and flooding.

$$\eta = 0.7272(1 - e^{-12/1708v_p}) \quad (9)$$

https://dx.doi.org/10.1021/acsomega.1c00009
ACS Omega 2021, 6, 8297−8307

4. PILOT TEST

4.1. Overview of the Pilot Site. The pilot test was conducted at well group I1 in Changqing YWL oilfield. This oilfield is located in the Ordos basin and characterized by low permeability and extreme heterogeneity. YWL was put into development in October 1996 with an inverted nine-spot rhombus pattern. After more than one decades' development, since 2008, the comprehensive water cut increased rapidly, and the monthly oil production rate quickly decreased. It is essential to apply profile control and oil displacement and maintain the oil production rate.

YWL is a typical low-porosity and low-permeability reservoir with a porosity of 12.64% and a permeability of 18.25 mD. The reservoir temperature was 55 °C, the viscosity of the underground crude oil was 1.95 mPa s, and the salinity of the formation water was 80,000 mg/L. The initial formation pressure of the YWL oilfield was 13.2 MPa. Well group I1 with one injection well and eight production wells, all of which were vertical, is shown in Figure 11. I1 was a water well, and P1 to P8 were oil wells. Other reservoirs and fluid properties are shown in Table 10.

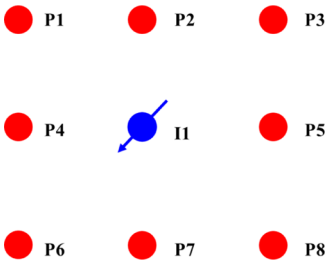

Figure 11. Well location of the pilot test well group.

Table 10. Reservoir and Fluid Properties

reservoir parameter	value
initial pressure	13.2 MPa
temperature	55 °C
oil density	0.763 g/cm^3
oil viscosity	1.95 mPa·s
saturation pressure	7.64 MPa
oil volume factor	1.297
water salinity	80,000 mg/L
water type	$CaCl_2$

4.2. Field Application. The porosity and permeability of the YWL block are 12.64% and 18.25 mD, respectively. The calculated diameter of the throat is 2.23 μm. Therefore, the minimum diameter of the PM applied to the YWL block is 100 nm as D_R could be 0.5 when PM100 achieved hydration equilibrium. PM100 had an excellent dispersion in injected water, and its particle size gradually increased with hydration time. Therefore, PM100 could smoothly inject into the reservoir and progressively migrate to the deep reservoir with injected water and achieved deep plugging.

Theoretical analysis and experimental evaluation showed that PM100 has good adaptability to YWL block and excellent plugging performance. The injection concentration is 0.5%, according to the relationship between the injection concentration and block rate. Also, the injection volume is about 12 tons. We assume that the best injection rate is consistent with a water injection rate of 40 m^3/d.

4.3. Performance Evaluation. Permeability variation between injection and production wells and pressure variation of injection wells before and after PM100 injection are analyzed to evaluate the blocking capacity of PM100.[35] We analyze the production difference of production wells after PM100 injection to verify PM100 profile control performance.

4.3.1. Injection Pressure. Researchers usually care about changing the injection pressure trend for injection wells, tubing pressure, and casing pressure. They also focus on the water injectivity presented by the daily water injection rate. To study the injection pressure trend after PM100 injection, we monitored tubing pressure and casing pressure during the injection process and also recorded the actual injection volume. The recorded values of injection pressure and injection volume during the injection process of PM100 are shown in Figure 12. We can find that during PM100 injection,

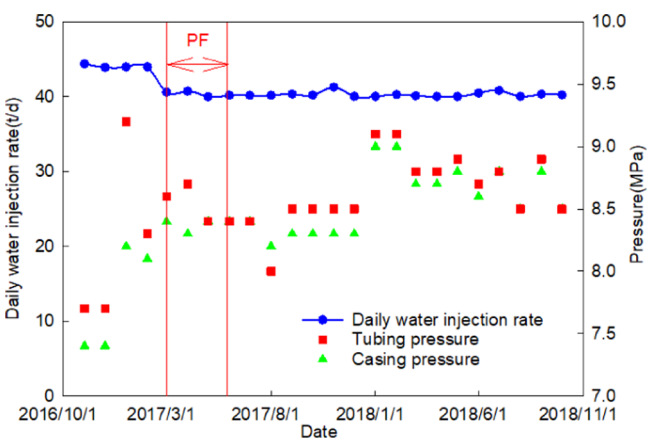

Figure 12. Injection pressure during the injection process of PM100.

there is no significant change in the injection volume, and it remained the same as an initial injection volume of 40 m^3/d, which indicated that the injection capacity does not decrease.

However, the tubing pressure and casing pressure show a significant increase. The results indicate that the injection well pressure will increase when the PM conformance control is effective. In the laboratory displacement experiment, the injection pressure will inevitably increase after the PMs form an effective block. In a laboratory displacement experiment, the water injection well corresponds to a production well, and the pressure will inevitably increase after the blockage is formed. Also, the field test found that the plug and the pressure increase will necessarily occur simultaneously.

Comparing before and after the microsphere injection, although the injection volume decreased by 5 m^3/d, the average injection pressure still increased from 7.4 to 8.7 MPa, which increased by 1.3 MPa that the PMs formed an effective plugging between the injection and production wells.

4.3.2. Permeability Between Injection-Production Wells. PM100 has good dispersion ability in formation water and can migrate to the deep formation to plug a high-permeability channel. When PM100 blocked the high-permeability channel, reservoir permeability decreased. After PM100 sealed the high-permeability channel, subsequent injected water flowed around the plugging area to expand the sweep volume; then, the permeability between injection and production wells decreased.

https://dx.doi.org/10.1021/acsomega.1c00009
ACS Omega 2021, 6, 8297−8307

Figure 13 shows permeability variation between injection and production wells before and after PM injection. It can be

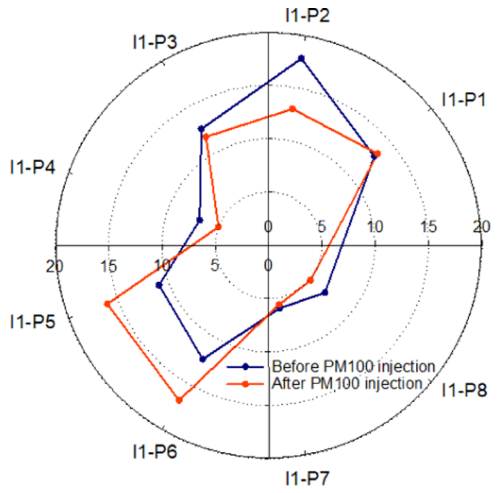

Figure 13. Interwell permeability before and after PM100 injection.

seen that interwell permeability of P2, P4, and P8 decrease from 17.76, 6.87, and 6.92 to 12.98, 5.00, and 5.13 mD, respectively. The injected PMs blocked the channel with high permeability between injection and production wells, resulting in a low-permeability area. Thus, the permeability between injection and production wells decreased.

However, the decrease in the permeability between the injection and production wells and the increase in oil production from the oil wells indicate that there is a blockage between the injection and production wells.

4.3.3. Oil Increase. Increased sweep efficiency leads to oil production increase. However, the plugging strength of microspheres is limited. When injection water broke through the plugging area, flow around injection water is not apparent, and the validity period of the PM is over. Three production wells show oil production variation. Therefore, the efficiency of PM100 flooding is 37.5%.

These production wells with permeability reduction between injection and production wells show good oil production performance. In this pilot test of PM deep profile control, the total oil increase in production wells is 556 t and the validity period of P2, P4, and P8 is 180, 254, and 122 d, respectively, and during validity period, the total oil increase is 162 t, 214, 83 t, respectively, as shown in Figure 14. The daily oil production rate and its growth multiples are shown in Figure 15. By comparing the daily oil production rate before and after PM100 injection, the daily oil production of P2 increased from 3.63 to 5.56, P4 increased from 0.56 to 1.39, and P8 increased from 6.12 to 6.56. The growth multiples are 1.53, 2.48, and 1.09.

5. CONCLUSIONS

By evaluating the swelling properties and plugging properties of PM100 and PM800, an accurate matching coefficient of the reservoir and PM based on the relationship between the blocking rate and CR is presented to choose the most appropriate PM size. We gain the optimal injection concentration and injection volume by the blocking rate. According to the new size selection method and injection parameter optimal method, we choose PM100 as the flooding agent to carry out a pilot test. The wells' performance is

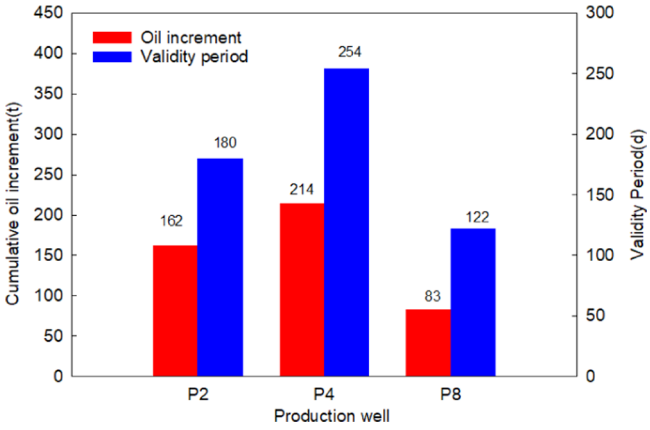

Figure 14. Oil increase and validity period of production wells.

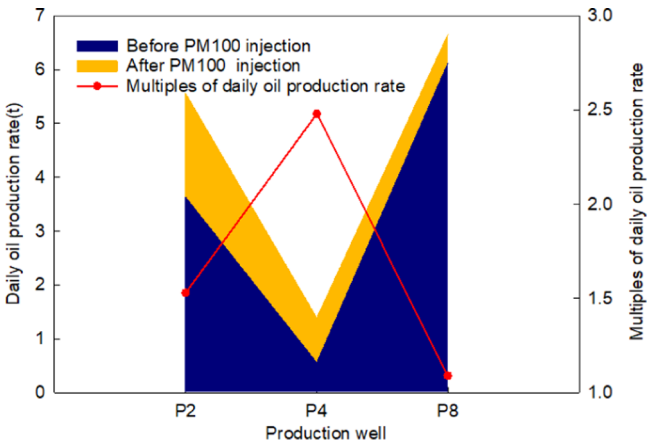

Figure 15. Daily oil production rate and multiples of production wells.

evaluated, including interwell permeability, oil increase, injectivity, and injection pressure well. According to this study, the following conclusions are drawn:

(1) PM100 and PM800 are easy to dissolve in water with the expansion ratio of water absorption being 6.9 and 4.2, respectively, and the solution has good stability and centralized size distribution.

(2) The new matching method between the reservoir and PM is established based on the relationship between the blocking rate and C_R. When C_R is 0.5, the PM conformance control can show the best plugging performance.

(3) According to the displacement results, the blocking rate is increased by injection concentration and stabilized. A similar trend is presented between the injection volume and plugging rate. The optimal injection concentration is 0.5%, and the optimal injection volume is 0.3 PV.

(4) The field application of PM100 presents a good performance. The success rate of profile control is 37.5%, the validity period is more than 120 days, and the daily oil production rate increased 1.7 times. However, the injection pressure shows no significant fluctuation, which indicates that the injection well pressure does not necessarily increase when the profile control is effective.

https://dx.doi.org/10.1021/acsomega.1c00009
ACS Omega 2021, 6, 8297−8307

AUTHOR INFORMATION

Corresponding Author

Tongjing Liu − *The Unconventional Oil and Gas Institute, China University of Petroleum (Beijing), Beijing 102249, China;* orcid.org/0000-0001-6763-2203; Phone: +8601089732158; Email: ltjcup@cup.edu.cn

Authors

Wenyue Zhao − *The Unconventional Oil and Gas Institute, China University of Petroleum (Beijing), Beijing 102249, China;* orcid.org/0000-0002-4340-289X

Juan Ni − *The Unconventional Oil and Gas Institute, China University of Petroleum (Beijing), Beijing 102249, China*

Ganggang Hou − *The Unconventional Oil and Gas Institute, China University of Petroleum (Beijing), Beijing 102249, China*

Yuqin Jia − *Oil & Gas Technology Research Institute of Changqing Oilfield Company, CNPC, Xi'an 710000, China*

Pengxiang Diwu − *College of Science, China University of Petroleum (Beijing), Beijing 102249, China*

Xinyu Yuan − *The Unconventional Oil and Gas Institute, China University of Petroleum (Beijing), Beijing 102249, China*

Jirui Hou − *The Unconventional Oil and Gas Institute, China University of Petroleum (Beijing), Beijing 102249, China*

Complete contact information is available at: https://pubs.acs.org/10.1021/acsomega.1c00009

Notes

The authors declare no competing financial interest.

ACKNOWLEDGMENTS

This research was financially supported by National Science and Technology Major Projects (2017ZX05009004).

REFERENCES

(1) Wang, Z. Analysis of Water Injection Development Process and Technology in Low Permeability Oilfield. *Med. Chem. Res.* **2019**, *03*, 152−154.

(2) Cao, X. *The Influence of Water Injection Development On the Heterogeneity of Extra Low*. Applied Research; Xi'an Shiyou University, 2017.

(3) Fan, Z.; Cheng, L.; Geng, C.; Tang, Y.; Wang, H. A New Approach for Heterogeneity Evaluation and Well Pattern Adjustment in Low Permeability Rerservoir. *Pet. Drill. Tech.* **2013**, *41*, 93−98.

(4) Pang, Z.; Li, Y.; Wang, B.; Huang, C.; Duan, W.; Yao, Z. Analysis of Influence Factors of Oil Displacement Efficiency in Ultra-Low Permeability Reservoir. *Unconv. Oil Gas* **2017**, *4*, 76−81.

(5) Wan, K.; Han, L.; Liu, Y.; Yang, Z. Characteristics and Influence Factors for Oil Displacement Efficiency by the Micro-Model Water Flooding Experiment in Low Permeability-Ultra Low Permeability Reservoir. *Petrochem. Ind. Appl.* **2016**, *35*, 103−112.

(6) Li, X. Analysis On Reservoir Characteristics and Formation Mechanism of Low Permeability Reservoir. *J. Changzhou Univ., Nat. Sci. Ed.* **2015**, *27*, 39−44.

(7) Wang, D. W.; Fang, J. K.; Liu, X. M.; Zhang, J. F.; Shu, D. W.; Zhang, X. Q. Preparation of Colored Polymer Microspheres and Research Progress Thereof in Textile Dyeing and Printing. *J. Text. Res.* **2019**, *40*, 175−182.

(8) Wang, H.; Lin, M.; Chen, D.; Dong, Z.; Yang, Z.; Zhang, J. Research On the Rheological Properties of Cross-Linked Polymer Microspheres with Different Microstructures. *Powder Technol.* **2018**, *331*, 310−321.

(9) Wang, B.; Lin, M.; Guo, J.; Wang, D.; Xu, F.; Li, M. Plugging Properties and Profile Control Effects of Crosslinked Polyacrylamide Microspheres. *J. Appl. Polym. Sci.* **2016**, *133*, 43666.

(10) Lin, M.; Zhang, G.; Hua, Z.; Zhao, Q.; Sun, F. Conformation and Plugging Properties of Crosslinked Polymer Microspheres for Profile Control. *Colloids Surf., A* **2015**, *477*, 49−54.

(11) Wu, T.; Zheng, M.; Zhou, Z.; Yang, H.; Cao, R. New Method for Plugging Performance Evaluation of Polymeric Nanospheres in Low Permeability Reservoir. *Fault-Block Oil Gas Field* **2018**, *25*, 498−501.

(12) Zheng, M.; Shen, H.; Wang, B.; Zhao, H.; Chen, G.; Yang, X.; Wang, X.; Zhang, P.; Wang, G. Polymer Nanospheres Control and Flooding in Low Permeability Oil Fields and Effects. *Petrochem. Ind. Appl.* **2012**, *31*, 32−36.

(13) Liu, W.; Zheng, Y.; Tie, L.; Xu, G.; Li, X.; Zhang, B. Experimental Study On Effects of Injection Mode of Polymer Microsphere/Surfactant Compound System On Profile Control. *Chem. World* **2018**, *59*, 598−603.

(14) Shen, H.; Ma, X.; Liu, P.; Wang, B.; Cao, L.; Zhang, P.; Chen, G. A Low Permeability Reservoir Polymer Microspheres to Improve Oil Recovery Technology Practice. *Petrochem. Ind. Appl.* **2016**, *35*, 44−48.

(15) Zhao, Y.; Li, S.; Zhang, W.; Jing, W.; Fang, H. Effect Evaluation of Polymer Microspheres Profile Control in Chi 46 Chang 8 Reservoir. *Petrochem. Ind. Appl.* **2018**, *37*, 84−88.

(16) Tian, Y.; Yi, Y.; Li, Z.; Bi, T.; Nan, Y. Application and Effect Analysis of Polymer Microsphere in Ansai Oilfield. *Chem. Eng. & Equip.* **2018**, *07*, 98−100.

(17) Liao, C. Research On the Adaptability of Polymer Elastic Microsphere Profile Control in Fang169 Fault Block. *China Petrol. Chem. Ind.* **2016**, *249*.

(18) Liu, F.; Chen, W.; Wu, Q.; Hua, C.; Lin, G. Analysis of Multiple Rounds Profile Control Effect of F8 Well Group in Suizhong 36-1 Oilfield. *Petrochem. Ind. Appl.* **2016**, *35*, 37−40.

(19) Wang, Y. *Experimental Study On Deep Profile Control and Flooding with Micro-Nano Microsphere in Pubei Oilfield*; Northeast Petroleum University, 2013.

(20) Pu, W.; Zhao, S.; Wang, L.; Mei, Z.; Feng, T.; Wei, B. Investigation Into the Matching Between the Size of Polymer Microspheres and Pore Throats. *Pet. Geol. Recovery Effic.* **2018**, *25*, 100−105.

(21) Liang, S.; Lu, X.; Liang, D.; Wen, H. A Study On Matching Relationship of Polymer Microsphere Size. *J. Southwest Pet. Univ., Sci. Technol. Ed.* **2016**, *38*, 140−145.

(22) Li, J.; Niu, L.; Lu, X. Migration Characteristics and Deep Profile Control Mechanism of Polymer Microspheres in Porous Media. *Energy Sci. Eng.* **2019**, *7*, 2026−2045.

(23) Yang, H.; Kang, W.; Yin, X.; Tang, X.; Song, S.; Lashari, Z. A.; Bai, B.; Sarsenbekuly, B. Research On Matching Mechanism Between Polymer Microspheres with Different Storage Modulus and Pore Throats in the Reservoir. *Powder Technol.* **2017**, *313*, 191−200.

(24) Gao, J. *The Matching Experiment of Deep Profile Control System and Reservoir Permeability in Gel Microcapsules*. Applied research; Northeast Petroleum University, 2016.

(25) Chen, Z. *Research On the Matching Relation Between the Diameter of Elastical Particle and Permeability of the Formation*. Applied research; Chin University of Petroleum: East China, 2016.

(26) Jia, Y.; Haien, Y.; Cheng, C.; Li, Z.; Hou, G.; Yuan, X.; Zhao, W.; Zhang, Z.; Liu, T. Field Application and Performance Evaluation of Polymer Microsphere Profile Control in Low Permeability Oil Reservoir. *Abu Dhabi International Petroleum Exhibition & Conference. Abu Dhabi*, 2019.

(27) Xie, K.; Cao, B.; Lu, X.; Jiang, W.; Zhang, Y.; Li, Q.; Song, K.; Liu, J.; Wang, W.; Lv, J.; Na, R. Matching Between the Diameter of the Aggregates of Hydrophobically Associating Polymers and Reservoir Pore-Throat Size During Polymer Flooding in an Offshore Oilfield. *J. Pet. Sci. Eng.* **2019**, *177*, 558−569.

(28) Xie, K.; Lu, S.; Pan, H.; Han, D. Analysis of Dynamic Imbibition Effect of Surfactant in Microcracks of Reservoir at High

Temperature and Low Permeability. *SPE Production & Operations* **2018**, *33*, 596.
(29) Chen, X.; Li, Y.; Liu, Z.; Zhang, J.; Chen, C.; Ma, M. Investigation On Matching Relationship and Plugging Mechanism of Self-Adaptive Micro-Gel (Smg) as a Profile Control and Oil Displacement Agent. *Powder Technol.* **2020**, *364* 774 DOI: 10.1016/j.powtec.2020.02.027
(30) Liang, S.; Hu, S.; Li, J.; Xu, G.; Zhang, B.; Zhao, Y.; Yan, H.; Li, J.J. . Study On Eor Method in Offshore Oilfield: Combination of Polymer Microspheres Flooding and Nitrogen Foam Flooding. *J. Pet. Sci. Eng.* **2019**, *178*, 629−639.
(31) Zhao, S.; Pu, W.; Wei, B.; Xu, X. A Comprehensive Investigation of Polymer Microspheres (Pms) Migration in Porous Media: Eor Implication. *Fuel* **2019**, *235*, 249−258.
(32) Pu, W.; Zhao, S.; Wang, S.; Wei, B.; Yuan, C.; Li, Y. Investigation Into the Migration of Polymer Microspheres (Pms) in Porous Media: Implications for Profile Control and Oil Displacement. *Colloids Surf., A* **2018**, *540*, 265−275.
(33) Li, R. *Performance Assessing of Cross-Linked Polyme Compound Microspheres and Surfactant Compound Profile Modification*. Applied research; China University of Petroleum: Beijing, 2015.
(34) Yang, H.; Kang, W.; Liu, S.; Bai, B.; Zhao, J.; Zhang, B. Mechanism and Influencing Factors On the Initial Particle Size and Swelling Capability of Viscoelastic Microspheres. *J. Dispersion Sci. Technol.* **2015**, *36*, 1673−1684.
(35) Bo, X. U.; Taiyu, L. I.; Yue, M.; Chao, L.; Wenchao, W. U.; Ping, L. I.; Qiang, L. Practical Application and Effect Evaluation of Polymer Microsphere Profile Control and Flooding Technology. *Petrochem. Ind. Appl.* **2019**, *38*, 71−75.

https://dx.doi.org/10.1021/acsomega.1c00009
ACS Omega 2021, 6, 8297−8307